On the use of oscillating jet flames in a coflow to develop soot models for practical applications

Agnes Jocher[a,*], Michael J. Evans[b], Paul R. Medwell[b], Bassam B. Dally[b], Heinz Pitsch[c], Graham J. Nathan[b]

[a] *Department of Chemical Engineering, Massachusetts Institute of Technology, Cambridge, MA, USA*
[b] *School of Mechanical Engineering, Centre for Energy Technology, The University of Adelaide, Adelaide, Australia*
[c] *RWTH Aachen University, Institute for Combustion Technology, Aachen, Germany*

Abstract

Oscillating jet flames in a coflow mimic certain features of turbulent flows in a simplified and controllable way. Our study aims to identify the potential of the HMOM soot model, which is validated in steady laboratory flames to be applied in practical, mostly turbulent flames. The model is found to accurately predict all the measurement parameters in a steady laminar sooting jet flame of ethylene/nitrogen mixture. When applied to an oscillating flame with the same fuel mixture, it was found that, while velocity, temperature, and OH fields are well predicted, the peak soot volume fraction is over predicted and occurs away from the experimentally measured location. The potential for soot model improvement is analysed by correlating the transient gas-phase species, polycyclic aromatic hydrocarbon, and soot formation or destruction behaviour. A need for improved soot nucleation, condensation, and oxidation formulations is identified. It is further found that the soot

*Corresponding author:
Email address: ajocher@mit.edu (Agnes Jocher)

number density distribution in mixture fraction space is comparable to the transitional turbulent flame regime dominated by Kelvin-Helmholtz rollers.

Keywords: non-premixed flame, soot, acoustic forcing

1. Introduction

Understanding soot particle formation and oxidation remains a major challenge in the field of combustion. Significant advances have been achieved in the last decades, but the processes leading to the formation and oxidation of soot are not yet fully understood. Continuing progress in computer power allows the development of more sophisticated soot models. While empirical or semi-empirical soot models provide reasonable agreement with experimental measurements, they do not thoroughly model the detailed physical and chemical processes involved in soot formation. High-fidelity soot and combustion models have been designed to account for some of these processes [1–3]. Another critical assumption is that soot models developed in steady laminar flames can reasonably be applied to real-world combustion systems. Due to the complexity of turbulent combustion environments, it is difficult to assess the validity of this assumption. Therefore, several studies have used non-premixed, oscillating jet flames in a coflow expecting to mimic turbulent flow features in a simplified and better controllable way [4–6].

In comparison with steady flames in a coflow, oscillating jet flames introduce additional flow time scales, which allows the assessment of the predictive quality of models under dynamic flow and strain. At the same time, the flame is complex enough to account for effects such as curvature and variation in residence times by oscillation, which is not the case in simpli-

fied one-dimensional or steady configurations that are often used to evaluate soot models [7]. For example, soot formation can depend on the characteristic time governing the chemistry of each gas-phase species when the characteristic times of kinetics and mixing are similar, in addition to the operating conditions [8].

In sooting oscillating flames, time-dependent effects are expected to be of importance due to slow rates of polycyclic aromatic hydrocarbon (PAH) formation and soot inception [8]. These formation and inception processes might then decouple from mixture fraction and result in strong sensitivities to flow-field dynamics [9] and eventually a phase-lag between oscillations and the response of the flame [5]. On the other hand, soot oxidation is a comparatively fast process expected to follow flow field dynamics.

Our preceding study with detailed chemistry focused on the performance of the Hybrid Method of Moments (HMOM) high-fidelity soot model [10] in comparison with Time-Resolved Laser-Induced Incandescence (TiRe-LII) [5] measurements in a steady and two forced ethylene coflow flames. While the computed and measured peak soot volume fraction agreed within a factor of two, a detached fuel pocket that was observed in the experiment was not predicted. New measurements and a computational study of forced laminar coflow flames, which includes the fuel plenum [6], show that to reliably simulate the experimental forcing conditions, the inlet velocity profile of the fuel flow should be described as a sum of sinusoids rather than using a parabolic, time-dependent function [4, 5].

Having certainty on the flow-field dynamics, the present study provides a time-scale analysis of flow-chemistry-soot interaction identifying the role of

condensation processes and oxidation rates. Additionally, soot distribution in oscillating flames is compared with steady and turbulent flames to shed more light on the question, how oscillating flames in a coflow can be used to bridge the gap in soot modelling between steady laminar and turbulent flames.

2. Computational methods and setup

Building on previous work and due to the available data set, in this study we selected experimental measurements obtained from a coannular axisymmetric coflow jet burner [6, 11, 12]. The fuel tube has an inner diameter of 5.6 mm and the coflow is injected through a concentrically aligned annulus of 74 mm in diameter. The fuel flow can be acoustically excited through a loudspeaker superimposing sinusoidal pressure perturbations at 10 Hz. The relatively low forcing frequency has been chosen to maximize the flame oscillation amplitude. Earlier studies found that jet flames in a coflow oscillate extensively at lower frequencies that are close to the observed natural flame oscillation frequency [13] but resemble steady jet flames when forced at higher frequencies [5].

To avoid flame smoking under forcing conditions, the fuel stream (41.7% ethylene, 58.3% nitrogen by volume) was adjusted to a total flow rate of 0.31 standard litres per minute (SLPM), corresponding to a bulk exit velocity of 0.21 m/s (Re = 104). Layers of glass beads between a pair of honeycombs were used to generate a uniform plug flow velocity profile of 0.23 m/s for the coflowing air. The experiments were computationally reproduced with detailed, two-dimensional, axisymmetric numerical simulations, similar to

those described in Jocher et al. [5]. A parallelized in-house code called CIAO was used to solve the Navier-Stokes equations in the low Mach number limit utilizing spatial and temporal staggering, together with Crank-Nicolson type time advancement [14]. Diffusion is approximated by the Curtiss-Hirschfelder approach [15] and mass conservation is accounted for with a correction velocity. Soret diffusion is considered, while the Dufour process is neglected. A time-implicit backward difference method, like implemented in CVODE [16] is used by the chemistry operator. The chemical mechanism [17, 18], containing 158 species, has been chosen due to its validation for a large set of fuels ranging from methane to iso-octane and one-ring aromatics using different configurations such as homogeneous auto-ignition, laminar premixed flames and diffusion flames. Furthermore, the mechanism has been used to validate the HMOM soot model in simulations of high temperature premixed ethylene flames, premixed benzene flames, an acetylene counterflow diffusion flame, toluene pyrolysis in shock-tubes, and a set of premixed ethylene flames exhibiting the bell-shaped dependence of soot volume fraction with temperature [19]. Gas-phase and soot radiation was implemented with a discrete ordinates method (DOM) [20] including CO_2, CO, and H_2O as radiating gas-phase species. The Hybrid Method of Moments (HMOM) [21] predicts soot quantities by taking the volume and surface of the soot particles into account. Source terms that govern the soot production evolution were employed for the processes of nucleation, condensation, surface growth, coagulation, oxidation, and fragmentation [22, 23]. The soot Number Density Function (NDF) was obtained by solving transport equations for a set of moments including the source terms mentioned above and accounting for thermophoretic effects.

Molecular diffusion of soot particles was neglected due to the typically low mass diffusivity or high Schmidt number of soot transport [24]. While the removal of particles from the population during oxidation has been a long-standing point of debate with the Method of Moments, leading to either neglect [25] or crude modelling of the term [26], HMOM circumvents the issue by assuming that the number of primary particles in an aggregate is constant [27]. Mass removal from the gas-phase during particle inception and surface growth was accounted for by two-way coupling between the gas- and particulate-phase. The computational boundary conditions were matched to the experimental setup described above. The coflow was modelled as a uniform plug flow, while the fuel velocity temporal profile was set as the sum of sinusoids obtained from the simulations of the flow through the fuel plenum [6]. This approach has been shown to match the measured data while achieving reasonable simulation times.

In the axial and radial direction, the numerical domain extends to 111.5 mm and 37 mm, respectively. The vertical boundary on the free stream side of the domain follows free-slip conditions and the top boundary was designed as an outflow with zero gradient conditions. Symmetry conditions were set for the centreline and a non-uniform, two-dimensional, cylindrical mesh with control volume of 288 (z) $\times$ 156 (r). The grid was refined in the vicinity of the nozzle outlet section with a minimum resolution of 0.02 mm in radial and axial directions. Further refinement was also applied in regions of high temperature gradients and soot formation. The starting point of the computational domain is defined to be the surface of the fuel tube. This is reasonable because the flame is slightly lifted, so that any heat transfer to

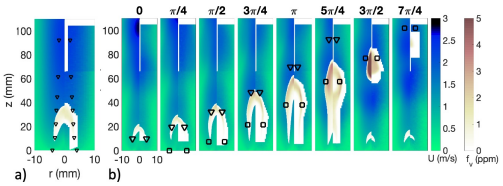

Figure 1: Velocity and soot volume fraction fields for the steady a) and oscillating b) flame. The left half of each panel shows the simulation results and the right half the experimental measurements by Foo et al. [11]. Within the white regions velocity measurements have a higher level of uncertainty due to interference from the soot. The downward facing triangles represent the instantaneous location of a massless, inert particle that follows the convective pathlines through the steady and oscillating flame, respectively, where the first soot volume fraction above the burner surface is detected in the experiment. The squares represent the pathlines where the peak soot volume fraction is detected in the experiment. For b) the images are displayed in 12.5 ms intervals corresponding to separating one oscillation cycle into eight phases with 45° phase angle difference.

the burner is small.

The incoming flow temperature is set constant to 294 K and the pressure is kept at atmospheric conditions. The computed forced flame was initialized with the steady flame computation and a start-up transient analysis confirmed the fully periodic state after seven oscillation cycles [28]. The simulation timestep was kept below 3.2×10^{-5} s.

3. Results and discussion

3.1. Computational results

The accuracy of the simulations in predicting the characteristics and soot formation was determined for both the steady and time-dependent flames. For the steady flame, agreement in magnitude and shape between the mea-

sured and computed two-dimensional velocity, soot volume fraction, and temperature fields is shown in Fig. 1 a) and Fig. S1-S10. The pathlines obtained by tracking a massless inert particle along the convective pathline through the location of the peak soot volume fraction overlap along the centreline for both the experiment and the simulation. Similarly, the measured location of the peak Planar Laser-Induced Fluorescence signal of the hydroxyl radical (OH-PLIF) agrees with the location of the simulated peak OH mass fraction, Fig. S8. Along the centerline, the source terms for soot condensation and surface growth peak with comparable magnitudes but at different heights above the burner surface (HAB), Fig. S3. Along the pathline in the wings of the flame, surface growth is the dominant source term for soot formation, followed by the source term for soot condensation. The mixture fraction Z was calculated following earlier studies [6, 29], noting that the stoichiometric mixture fraction is Z_{st}=0.142.

For the oscillating flame, the measured temperature and OH-PLIF images as well as the flow velocity fields, measured using Particle Image Velocimetry (PIV) technique, agree with the computed temperature, OH mass fraction, and velocity fields, Fig. S14-S18. However, the peak soot volume fraction value, over one oscillation cycle, is over-predicted by a factor of about two, Fig. 1 b). Furthermore, the simulated peak soot volume fraction occurs on the centreline although experimental measurements locate the peak soot volume fraction in the wings of the flame, Fig. S16. Even though the simulated peak soot volume fraction is considerably higher than measured, the oxidation of the soot pocket is predicted faster than measured, as shown in phase angle $7\pi/4$ of Fig. 1 b) and Fig. S16. The experimental setup has an un-

certainty and lower limit of detection for the soot volume fraction of $\pm$ 0.03 ppm (1σ) and 0.01 ppm and is consistent with the steady flame study used for calibration [11]. Consequently, neither flow field mismatches nor measurement uncertainties can explain the observed discrepancies. Analysing the source terms that contribute over time to the simulated peak soot volume fraction reveals that condensation is dominating in the oscillating flame mainly due to contributions from acenaphthylene (A2R5-$C_{12}H_8$) and naphthalene (A2-$C_{10}H_8$), Fig. S11 and S12. In the employed soot model, both source terms for nucleation and condensation depend on the concentration of PAH dimers [1]. Due to the high collision frequency with other PAH dimers or larger soot particles, dimers are assumed to be in steady state. Therefore, any reduction in the condensation rate will lead to an increase of the nucleation source term and would keep the peak soot volume fraction overprediction roughly the same. This behavior could be different with the use of other nucleation/condensation models. For the present model, however, a reduction of the dimer concentration, assumed to form from self-collision of various gas-phase species ranging from naphthalene to cyclopenta[cd]pyrene (A4R5-$C_{18}H_{10}$), could lead to an improved prediction of the peak soot volume fraction in this flame. Most of the dominant rates for acenaphthylene and naphthalene formation at about 1500 K, the temperature at the peak soot volume fraction formation in the oscillating flame, are adapted from reactions with a single aromatic ring. Recent literature [30] for example, also reports an acenaphthylene and naphthalene overprediction for the used mechanism but suggests rates that better match experimental conditions.

3.2. Flow-chemistry-soot interaction

Concentrations of PAHs, like naphthalene, govern nucleation and condensation rates, while acetylene (C_2H_2) together with hydrogen concentration control the surface growth rates of soot particles. Bisetti et al. [24] found that naphthalene exhibits stronger unsteady effects than acetylene, due to a lower Damköhler number. Whether a similar behaviour can be expected for PAHs larger than naphthalene could not be assessed due to the reduced mechanism employed. In this work, the eight PAH species modelled to act as soot precursors are naphthalene (A2-$C_{10}H_8$), acenaphthylene (A2R5-$C_{12}H_8$), biphenyl (P2-$C_{12}H_{10}$), phenanthrene (A3-$C_{14}H_{10}$), acephenanthrylene (A3R5-$C_{16}H_{10}$), pyrene (A4-$C_{16}H_{10}$), fluoranthene (FLTN-$C_{16}H_{10}$), and cyclopenta[cd]pyrene (A4R5-$C_{18}H_{10}$). The naming conventions follow the nomenclature introduced by Frenklach et al. [31]. To assess transient species formation, the instantaneous maximum mass fraction in the oscillating flame was extracted and normalized by the corresponding value of the steady flame, Fig. 2 a-d). Smaller species, such as C_2H_2, respond faster to a rapidly changing scalar dissipation field due to their fast kinetics compared with PAHs, which have slower formation rates [2]. Consequently, the normalized values of smaller species in Fig. 2 a-b) deviate less from unity over one oscillation cycle than those of PAHs, Fig. 2 c-d). Figure 2 c-d) suggests that under the studied flame conditions, with the employed mechanism, the PAH growth rates do not scale directly with PAH size in the oscillating flame, while they do in the steady flame, Fig. S2. The reason behind this apparent contradiction is not yet well understood, so that further work is needed to explain it.

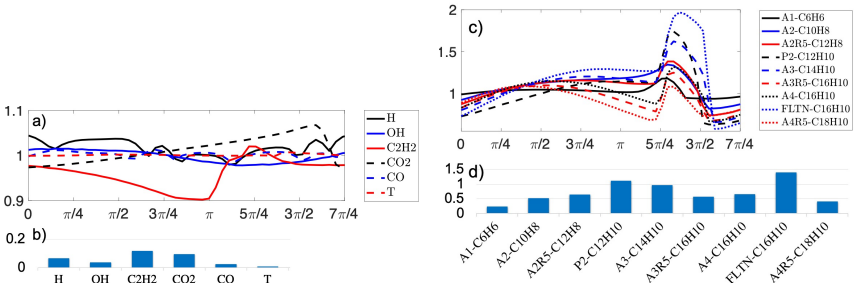

Figure 2: a) and c) Displays the maximum instantaneous species mass fractions and temperature over one oscillation cycle normalized with the corresponding maximum value in the steady flame. The bar diagrams b) and d) show the difference between the spatial maximum and minimum value for each species over one oscillation cycle displayed in a) and c).

Figure S15 and S16 show that, areas of peak temperature are outside regions with considerable soot volume fraction and therefore gas-phase and soot radiation do not significantly reduce the peak temperature over one cycle. In addition, peak concentrations of species such as OH, which participate in chemical reactions with substantial heat release, remain quite constant during flame oscillation, Fig. 2 a-b). Thus, almost no deviation from unity can be observed for normalized, instantaneous peak temperature.

In Figure 3, the maximum instantaneous growth rates for soot volume fraction in the oscillating flame are normalized by the corresponding values in the steady flame. Following the trends in Fig. 2 the surface growth rate $\hat{k}_{surf}$, mainly due to the C_2H_2 concentration, exhibits smaller transient effects than for example the combined nucleation $\hat{k}_{nuc}$ and condensation $\hat{k}_{cond}$ rate governed by PAH concentrations. Soot oxidation $\hat{k}_{ox}$ seems to be affected by the flame oscillation and deviates from unity at a phase angle of $3\pi/2$. In comparison with the PAHs, the gas-phase species directly involved

in soot oxidation, such as OH and O_2 appear relatively unaffected by flame oscillation. Yang et al. [3] found that for a non-premixed C_2H_4/air flamelet solution using the HMOM soot model the oxidation process is considerably faster than surface growth or the combined nucleation and condensation process. Nevertheless, the non-negligible deviation from unity of $\hat{k}_{ox}$ suggests that soot oxidation is observably slower than OH formation. The peak value of the soot oxidation rate is observed at a phase angle of $3\pi/2$ in the tip of the detached fuel pocket at 83 mm HAB, Fig. S12. At these conditions the O_2 mass fraction is about an order of magnitude larger than the OH mass fraction while in the steady flame and other phase angles of the oscillating flame OH and O_2 mass fractions are comparable at peak soot oxidation rates, Fig. S19-S21. In addition, the fluid temperature reaches 1673 K which is at least 100 K lower than in other phase angles, or in the steady flame at peak soot oxidation rates. Therefore, while peak temperature deviation over one oscillation cycle is found to be small, the variation in local temperatures between cycles might be non-negligible. In the HMOM model soot particles react with OH using the collision limit rate with a reaction probability of 0.13 identified by Neoh et al. [32]. Under their experimental conditions Neoh et al. identified OH to be the dominant oxidant but mention that O_2 can become a significant factor particularly at lower temperatures. For soot particle oxidation with O_2 the rate by Kazakov et al. [33] is used. Recently, Guo et al. [34] analyzed soot oxidation measurements and model rates from the literature and found that the predicted model rates are generally higher than measured. The current results support the findings by Guo et al. Optimized rate expressions for soot oxidation by OH and O_2 as provided by Guo et

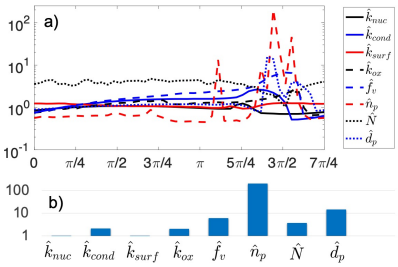

Figure 3: Displays the maximum instantaneous growth rates for the total soot volume moment $M_{1,0}$ for soot particle nucleation $\hat{k}_{nuc}$, condensation $\hat{k}_{cond}$, surface growth $\hat{k}_{surf}$, and oxidation $\hat{k}_{ox}$ as well as maximum instantaneous values of soot volume fraction $\hat{f}_v$, number of primary particles $\hat{n}_p$, number density $\hat{N}$, and primary particle diameter $\hat{d}_p$ over one oscillation cycle normalized with the corresponding maximum value in the steady flame. The bar diagram b) shows the difference between the spatial maximum and minimum value over one oscillation cycle displayed in a).

al. [34] or detailed, sterically-resolved modeling of soot oxidation [35] could improve the simulated oxidation rates. The number of primary soot particles $\hat{n}_p$ is expected to originate mainly from nucleation [2]. However, Fig. 3 shows a considerable peak at $3\pi/2$ while $\hat{k}_{nuc}$ is minimal. A two-dimensional plot (Fig. S13) reveals that the number of primary soot particles peaks at the bottom of the pinched off soot pocket, shown in Fig. 1, where soot oxidation is the dominant source term. The number of primary soot particle fields shown in Fig. S13 suggests that the large value is a consequence of numerical inaccuracies. This observation is supported by Fig. S12 where fragmentation is found to be negligible.

3.3. Soot characteristics in mixture fraction space

In the preceding section, the spatio-temporal inhomogeneities and hierarchies for various fields have been discussed by analysing one oscillation cycle.

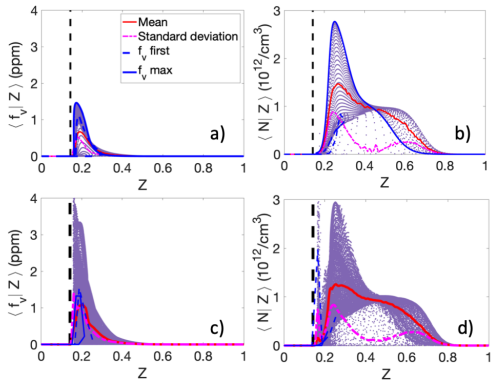

Figure 4: Soot volume fraction and number density conditioned on mixture fraction in the steady (a) and b) and oscillating flame (c) and d). The scatter plot (purple dots) displays the steady flame and instantaneous fields of the oscillating flame. The dashed line, labelled with "f_v first" in the legend, shows the conditions tracked along the pathline through the location of the measured first soot occurrence in the experiment. The thick solid line, labelled with "f_v max" in the legend, shows the conditions tracked along the pathline through the location of the measured peak soot occurrence in the experiment. The vertical dashed line indicates the location of the stoichiometric mixture fraction.

Similar to observations in direct numerical simulations (DNS) of sooting turbulent flames [2], soot fields have been shown to display the most significant spatial variability compared with temperature, gas-phase species, and PAH variations. In this subsection, soot statistics in mixture fraction space will be analysed comparing the steady and oscillating flame to better identify which parameter fields in oscillating flames might allow for bridging the gap between steady and turbulent sooting flame modelling.

Figure 4 shows the soot volume fraction and number density conditioned on mixture fraction in the steady and oscillating flame. As noted for Fig. 1, the scatter plots show that the peak soot volume fraction in the oscillating flame (Fig. 4 c)) is higher than in the steady flame (Fig. 4 a)) but the soot distribution in mixture fraction space does not extend further into richer or leaner regions. The peak value of f_v max for the oscillating flame (Fig. 4 c)) is lower than suggested by the scatter because of the different maximum soot volume fraction locations in the experiment and the simulation. Here, the pathline through the location of the measured peak soot occurrence is displayed. For the steady flame f_v max is tracked through a region of pure fuel while for the oscillating flame a maximum mixture fraction of 0.24 is experienced. This can be seen as well for the f_v max profile in the number density figures. For both the steady and oscillating flame, the mean and standard deviation of the number density distribution are comparable in magnitude.

A similar trend in conditioned soot volume fraction distribution over mixture fraction space has been found for a sooting turbulent DNS by Attili et al. [2] at early simulation times of about 1 ms. At this early simulation time,

two non-premixed flames were not turbulent but started to develop into regions of high turbulence. Consequently, the f_v distribution in the presented oscillating flame in a coflow (Fig. 4 c)) is more comparable to the steady flame in a coflow (Fig. 4 a)) than to turbulent conditions. However, Attili et al. observed that at 1 ms the soot number density grows quickly with a single peak in the range of $0.2<Z<0.5$ due to the naphthalene concentration. In the current work, we observe a more complex number density distribution, for both the steady (Fig. 4 b)) and unsteady flame (Fig. 4 d)), which is similar to the transitional phase of the turbulent jet evolution by Attili et al. In the transitional phase, the flow is dominated by Kelvin-Helmholtz rollers and turbulence is not fully developed [2]. It has been shown that steady coflow jet flames can exhibit a natural flame oscillation triggered, for example, by a magnetic field exposure [36] that allows for modified Kelvin-Helmholtz instabilities to suddenly govern the flame dynamics. The 10 Hz frequency used to force the oscillating flame is close to the observed natural flame oscillation frequency [13], indicating that Kelvin-Helmholtz instabilities are a flame characteristic in these coflow flames that could relate to transitional flow and soot number density patterns in turbulent flames. However, even though both burner diameter and equivalence ratio have been shown to affect oscillation timescales in turbulent jet flames, typical frequencies for ethylene-air flames are above 600 Hz [37]. For oscillating flames, it has been shown that higher forcing frequencies reduce the flame response and the flame resembles a steady flame [5]. Forcing frequencies below 10 Hz, increase the likelihood that the flame will extinguish. The relatively high strain level in the neck of the present 10 Hz oscillating flame is consistent with high rates

of mixing-induced soot oxidation found in turbulent flames. Besides, regions of highest soot, within the detached flame, correspond to regions of lowest strain which is consistent with previous work on turbulent jet flames [6, 38].

4. Conclusions

The predicted velocity, temperature, and soot volume fraction fields in the steady coflow flame compare well with the experimental measurements. For the oscillating flame, the predicted time-dependent temperature, strain rate, and OH mass fraction profiles agree well with the experimental measurements, while the peak soot volume fraction is over predicted and located on the centreline instead of in the wings of the flame. Soot oxidation is predicted to occur faster than in the experiments, leading to negligible predicted soot volume fractions in locations where soot was still measured. The soot overprediction could be traced to dominant soot condensation rates, particularly to the acenaphthylene and naphthalene concentration in the gas-phase. It is shown that under the studied flame conditions, and with the employed mechanism, the PAH formation rates do not scale directly with PAH size and therefore larger PAHs do not necessarily exhibit stronger unsteady effects than do smaller PAHs. Even though the species involved in soot oxidation (OH, O_2) appear relatively unresponsive to the flame oscillation compared with PAHs, the oxidation source term shows a more transient behaviour than the condensation source term due to local changes in the flame temperature over an oscillation cycle. Finally, we observe that soot volume fraction distributions in mixture fraction space are very similar in the steady and oscillating flame but are quite different from transitional

or turbulent flame distributions. The soot number density distribution in mixture fraction space, however, can be compared in both, the steady and oscillating flame to the transitional regime dominated by Kelvin-Helmholtz rollers in a turbulent flame. This suggests that further improvements in the modelling could be obtained by improved soot nucleation and condensation rates to avoid over prediction of the peak soot volume fraction and reduced soot oxidation rates to match experimental measurements.

Acknowledgements

This research used resources of the National Energy Research Scientific Computing Center (NERSC), a U.S. Department of Energy Office of Science User Facility operated under Contract No. DE-AC02-05CH11231. Agnes Jocher acknowledges financial support from the DFG Research Fellowship under JO 1526/1-1.

References

[1] G. Blanquart, Chemical and statistical soot modeling, Ph.D. thesis, Stanford University (2008).

[2] A. Attili, F. Bisetti, M. E. Mueller, H. Pitsch, Formation, growth, and transport of soot in a three-dimensional turbulent non-premixed jet flame, Combust. Flame 161 (7) (2014) 1849–1865.

[3] S. Yang, J. K. Lew, M. E. Mueller, Large eddy simulation of soot evolution in turbulent reacting flows: Presumed subfilter pdf model for

sootturbulencechemistry interactions, Combust. Flame 209 (2019) 200–213.

[4] S. B. Dworkin, J. A. Cooke, B. A. Bennett, B. C. Connelly, M. B. Long, M. D. Smooke, R. J. Hall, M. B. Colket, Distributed-memory parallel computation of a forced, time-dependent, sooting, ethylene/air coflow diffusion flame, Combust. Theor. Model. 13 (5) (2009) 795–822.

[5] A. Jocher, K. Foo, Z. Sun, B. Dally, H. Pitsch, Z. Alwahabi, G. Nathan, Impact of acoustic forcing on soot evolution and temperature in ethylene-air flames, Proc. Combust. Inst. 36 (1) (2017) 781–788.

[6] K. K. Foo, M. J. Evans, Z. Sun, P. R. Medwell, Z. T. Alwahabi, G. J. Nathan, B. B. Dally, Calculated concentration distributions and time histories of key species in an acoustically forced laminar flame, Combustion and Flame 204 (2019) 189 – 203.

[7] C. R. Shaddix, J. E. Harrington, K. C. Smyth, Quantitative measurements of enhanced soot production in a flickering methane/air diffusion flame, Combust. Flame 99 (3-4) (1994) 723–732.

[8] A. Cuoci, A. Frassoldati, T. Faravelli, E. Ranzi, Formation of soot and nitrogen oxides in unsteady counterflow diffusion flames, Combustion and Flame 156 (10) (2009) 2010 – 2022.

[9] C. R. Shaddix, K. C. Smyth, Laser-induced incandescence measurements of soot production in steady and flickering methane, propane, and ethylene diffusion flames, Combust. Flame 107 (4) (1996) 418–452.

[10] M. Mueller, G. Blanquart, H. Pitsch, Hybrid Method of Moments for modeling soot formation and growth, Combust. Flame 156 (6) (2009) 1143–1155.

[11] K. K. Foo, Z. Sun, P. R. Medwell, Z. T. Alwahabi, G. J. Nathan, B. B. Dally, Influence of nozzle diameter on soot evolution in acoustically forced laminar non-premixed flames, Combust. Flame 194 (2018) 376–386.

[12] K. K. Foo, Z. Sun, P. R. Medwell, Z. T. Alwahabi, G. J. Nathan, B. B. Dally, Soot evolution and flame response to acoustic forcing of laminar non-premixed jet flames at varying amplitudes, Combust. Flame 198 (2018) 249–259.

[13] A. Jocher, J. Bonnety, T. Gomez, H. Pitsch, G. Legros, Magnetic control of flame stability: Application to oxygen-enriched and carbon dioxide-diluted sooting flames, Proc. Combust. Inst. 37 (2019) 5637–5644.

[14] O. Desjardins, G. Blanquart, G. Balarac, H. Pitsch, High order conservative finite difference scheme for variable density low Mach number turbulent flows, J. Comput. Phys. 227 (15) (2008) 7125–7159.

[15] T. P. Coffee, J. M. Heimerl, Transport algorithms for premixed, laminar steady-state flames, Combust. Flame 43 (1) (1981) 273–289.

[16] P. N. Brown, G. D. Byrne, A. C. Hindmarsh, VODE: A Variable-Coefficient ODE Solver, SIAM Journal on Scientific and Statistical Computing 10 (5) (1989) 1038–1051.

[17] G. Blanquart, P. Pepiot-Desjardins, H. Pitsch, Chemical mechanism for high temperature combustion of engine relevant fuels with emphasis on soot precursors, Combust. Flame 156 (3) (2009) 588–607.

[18] K. Narayanaswamy, G. Blanquart, H. Pitsch, A consistent chemical mechanism for oxidation of substituted aromatic species, Combust. Flame 157 (10) (2010) 1879–1898.

[19] G. Blanquart, H. Pitsch, Analyzing the effects of temperature on soot formation with a joint volume-surface-hydrogen model, Combust. Flame 156 (8) (2009) 1614–1626.

[20] F. Liu, H. Guo, G. J. Smallwood, Effects of radiation model on the modeling of a laminar coflow methane/air diffusion flame, Combust. Flame 138 (1-2) (2004) 136–154.

[21] M. E. Mueller, G. Blanquart, H. Pitsch, A joint volume-surface model of soot aggregation with the method of moments, Proc. Combust. Inst. 32 (1) (2009) 785–792.

[22] G. Blanquart, H. Pitsch, A joint Volume-Surface-Hydrogen muti-variate model for soot formation, in: Combustion Generated Fine Carbonaceous Particles, H. Bockhorn, A. D'Anna, A. Sarofim, and H. Wang, Eds. KIT Scientific Publishing, Karlsruher Institut für Technologie, 2009, pp. 439–466, 978-3-86644-441-6.

[23] M. E. Mueller, H. Pitsch, Large eddy simulation subfilter modeling of soot-turbulence interactions, Phys. Fluids 23 (11) (2011) 115104.

[24] F. Bisetti, G. Blanquart, M. E. Mueller, H. Pitsch, On the formation and early evolution of soot in turbulent nonpremixed flames, Combust. Flame 159 (1) (2012) 317–335.

[25] M. Frenklach, Method of moments with interpolative closure, Chem. Eng. Sci. 57 (12) (2002) 2229–2239.

[26] H. B. F. Mauss, B. Trilken, N. Peters, Soot Formation in Combustion - Mechanisms and Models, Springer-Verlag, 1994, Ch. Soot Formation in Partially Premixed Diffusion Flames at Atomspheric Pressure, p. 325.

[27] M. Mueller, G. Blanquart, H. Pitsch, Modeling the oxidation-induced fragmentation of soot aggregates in laminar flames, Proc. Combust. Inst. 33 (1) (2011) 667–674.

[28] S. Dworkin, B. Connelly, A. Schaffer, B. Bennett, M. Long, M. Smooke, M. Puccio, B. McAndrews, J. Miller, Computational and experimental study of a forced, time-dependent, methane–air coflow diffusion flame, Proc. Combust. Inst. 31 (1) (2007) 971–978.

[29] M. J. Evans, C. Petre, P. R. Medwell, A. Parente, Generalisation of the eddy-dissipation concept for jet flames with low turbulence and low damkhler number, Proc. Combust. Inst. 37 (2019) 4497–4505.

[30] T.-C. Chu, Z. J. Buras, P. Oßwald, M. Liu, M. J. Goldman, W. H. Green, Modeling of aromatics formation in fuel-rich methane oxy-combustion with an automatically generated pressure-dependent mechanism, Physical Chemistry Chemical Physics 21 (2) (2019) 813–832.

[31] M. Frenklach, W. Gardiner, S. Stein, D. Clary, T. Yuan, Mechanism of soot formation in acetylene-oxygen mixtures, Combustion Science and Technology 50 (1-3) (1986) 79–115.

[32] A. S. K.G. Neoh, J.B. Howard, Soot oxidation in flames, in: G. S. D.C. Siegla (Ed.), Particulate Carbon Formation During Combustion, PlenumPress, 1981, pp. 261–277.

[33] A. Kazakov, H. Wang, M. Frenklach, Detailed modeling of soot formation in laminar premixed ethylene flames at a pressure of 10 bar, Combustion and Flame 100 (1) (1995) 111 – 120.

[34] H. Guo, P. M. Anderson, P. B. Sunderland, Optimized rate expressions for soot oxidation by oh and o2, Fuel 172 (2016) 248 – 252.

[35] M. Frenklach, Z. Liu, R. I. Singh, G. R. Galimova, V. N. Azyazov, A. M. Mebel, Detailed, sterically-resolved modeling of soot oxidation: Role of o atoms, interplay with particle nanostructure, and emergence of inner particle burning, Combustion and Flame 188 (2018) 284 – 306.

[36] A. Jocher, H. Pitsch, T. Gomez, J. Bonnety, G. Legros, Combustion instability mitigation by magnetic fields, Phys. Rev. E 95 (2017) 063113.

[37] P. R. Knott, Noise generated by turbulent non-premixed flames., Ph.D. thesis, The Ohio State University (1969).

[38] S. Mahmoud, G. Nathan, Z. Alwahabi, Z. Sun, P. Medwell, B. Dally, The effect of exit strain rate on soot volume fraction in turbulent non-premixed jet flames, Proceedings of the Combustion Institute 36 (1) (2017) 889 – 897.